Observation of metallic sphere – complex plasma interactions in microgravity

M. Schwabe[1], S. Zhdanov[1], T. Hagl[1], P. Huber[1], A. M. Lipaev[2], V. I. Molotkov[2], V. N. Naumkin[2], M. Rubin-Zuzic[1], P. V. Vinogradov[3], E. Zaehringer[1], V. E. Fortov[2] and H. M. Thomas[1]

[1]Institut für Materialphysik im Weltraum, Deutsches Zentrum für Luft- und Raumfahrt (DLR), 82234 Weßling, Germany
[2]Joint Institute of High Temperatures, Russian Academy of Sciences, 125412 Moscow, Russia
[3]Rocket Space Corporation "Energia", 141070 Korolev, Moscow Region, Russia

E-mail: `mierk.schwabe@dlr.de`

Abstract. The PK-3 Plus laboratory on board the International Space Station is used to study the interaction between metallic spheres and a complex plasma. We show that the metallic spheres significantly affect both the local plasma environment and the microparticles. The spheres charge under the influence of the plasma and repel the microparticles, forming cavities surrounding the spheres. The size of the cavity around a sphere is used to study the force balance acting on microparticles at the cavity edge. We show that the ion drag force and pressure force from other microparticles balances with the electric force acting from the sphere to within 20%. At intermediate distances from the sphere surface, the interaction between the microparticles and the metallic spheres is attractive due to the drag force from the ions which are moving towards the highly charged spheres. The spheres thus strongly affect the plasma fluxes. This modification of the plasma flux can lead to an effective surface tension acting on the microparticles, and to the excitation of dust-density waves near the spheres, as the local electric field crosses a threshold.

PACS numbers: 52.27.Lw,52.35.Fp,52.35.Mw

Keywords: dusty plasma, complex plasma, dust density waves, cavitation, microgravity

1. Introduction

Dusty plasmas are plasmas that contain micro- or nanometer sized grains in addition to neutral atoms/molecules, ions, and electrons. They are ubiquitous and can, for instance, be found in space, in the atmosphere of the Earth, and in the laboratory [1]. In astrophysics, the influence of the dust component on the charge balance, dynamics, thermodynamics, and chemistry is crucial [1]. Furthermore, it has recently been realized

that charges of dust particles with sizes of submicron and up are important during the planet formation process [2–4]. An "electrostatic barrier" can hinder the dust growth [5]. Under certain conditions, the dust size distribution becomes bimodal, so that micro- and macrobodies interact [6]. In diffuse regions in the interstellar medium, the degree of ionization is much higher than in protoplanetary disks, and plasma-mediated interactions between polydisperse dust particles become important and might lead, for instance, to the formation of dusty clumps [7].

In this paper, we study a related subject: the interaction of metallic spheres of 1 mm diameter with microparticles immersed in a low temperature plasma under microgravity conditions. Low temperature plasmas that contain well-defined microparticles under laboratory conditions are termed *complex plasmas* in analogy with complex fluids [8, 9]. The microparticles collect ions and electrons from the plasma and acquire high negative charges, so that they interact via a screened Coulomb potential. They can be observed individually and thus enable observations on the kinetic level of diverse effects such as vortices, tunneling, crystallization fronts, various wave effects, and the onset of instabilities [10–18].

In ground experiments, gravity is one of the strongest forces acting on microparticles in a plasma, pulling them towards the lower plasma sheath, where they are suspended by the sheath's strong electric field. In this region, strong ion fluxes are present, which lead to effects such as wake formation [16, 19]. Thus, it is desirable to perform experiments under microgravity conditions, when they are suspended in the more homogeneous plasma bulk with a weak electric field [20]. In the present experiment, millimeter sized metallic spheres were injected into the plasma together with the microparticles. On the ground, it is next to impossible to study the interaction between charged microparticles and spheres for an extended period, as the spheres immediately drop to the ground. Microgravity makes such an investigation possible.

In the first experiments on complex plasmas in Earth orbit, the cosmonauts Pavel Vinogradov and Anatoly Soloviev shook an ampule containing charged microparticles on board the Mir space station in order to study the particles' trajectories [21].

Here we report on the last experiment of the PK-3 Plus laboratory on board the International Space Station (ISS) [22–24]. The laboratory was operated on the space station from 2006 to 2013. Its heart consisted of a radio-frequency plasma chamber with an electrode distance of 3 cm and electrodes of diameter 6 cm, surrounded by grounded guard rings, see figure 1. Dispensers mounted in the guard rings were filled with microparticles of various sizes and metallic spheres of 1 mm diameter. By shaking the dispensers, microparticles were injected into the plasma. Typically, the spheres were held inside the dispensers by sieves. Then, large symmetric microparticle clouds formed in the plasma bulk. The weightless microparticle clouds typically contain a central particle-free region called "void". Its formation is governed by the interplay between the ion drag and electric forces acting on the microparticles [20]. It is possible to change the ratio of these forces and thus close the void, for instance by reducing the discharge power [25].

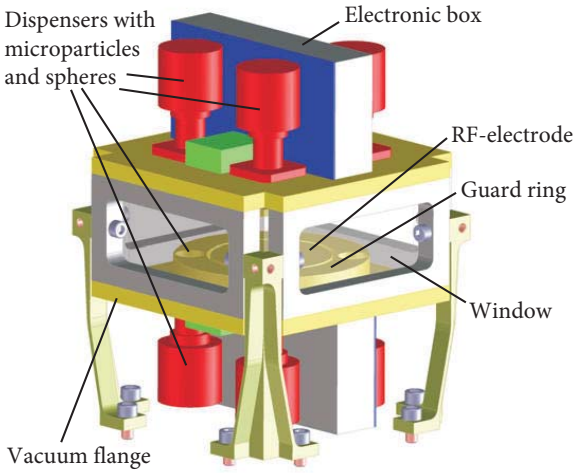

Figure 1. Sketch of the setup of the radio-frequency plasma chamber at the heart of the PK-3 Plus Laboratory. Adapted from [22].

The PK-3 Plus Laboratory has been used to study a diverse range of topics by investigating the microparticle dynamics, for instance electrorheological plasmas [26], wave excitation [27], lane formation [28], instabilities [29], phase transitions [30], turbulence [18, 31], and wave transmission across interfaces [32].

The goal of the experiment presented here was to study, for the first time, the interaction between macroscopic objects and microparticles immersed in a plasma in microgravity. By investigating gravitationally and electrically floating macroscopic bodies as opposed to fixed probes or surfaces, we are able to use the natural motion of the macrobodies through the complex plasma cloud and the microparticles' response to extract information on the effect of the complex plasma on the spheres and vice versa. The long interaction time made possible by microgravity and the large charges acquired by the relatively big spheres increase the magnitude of the observed effects.

For the purpose of this experiment, the dispensers were shaken so rigorously that the metallic spheres of 1.00 ± 0.01 mm diameter that were present inside the dispenser broke through the sieve and entered the argon plasma together with the remaining microparticles. Steel spheres were selected because of their durability and small sticking probability of surrounding microparticles. In a first-order approximation, the material of the spheres is unimportant for the interactions of the spheres with the microparticles and the plasma – metallic, dielectric and semiconductor spheres will all attain floating potential when exposed to the plasma. Secondary effects such as secondary electron emission depend on the material [33, 34], but are beyond the scope of the present paper to take into account.

It was again cosmonaut Pavel Vinogradov who performed the experiment, and, as in the very first experiment on complex plasmas in Earth orbit, he shook the experimental container to impart momentum on the particles inside. While the effect of the shaking on the microparticles was minimal in PK-3 Plus because of the strong confinement,

it was essential to impart momentum on the metallic spheres, which were accelerated when a chamber wall hit them.

The interaction of additional objects with complex plasmas has been studied regarding probes/wires [35–40], projectiles moving through the cloud [41–44], and 3D shaped substrates or perpendicular walls at different potentials [45, 46]. When the object is electrically floating or biased negatively, microparticle-free regions ("cavities") with a sharp edge form around the object. In these cavities, the force balance is opposite to that of the void: The microparticles are repelled from negatively charged objects, and ion drag pushes microparticles towards the objects, whereas the void is formed because ions push the microparticles outwards and the discharge electric field inwards. There can also be microparticle circulation induced by the objects [35, 47]. Samsonov et al. [37] found that near particles are repelled, as close to the object the electric repulsion prevails, and far particles are attracted as they follow the ion drag. Usachev et al. [48] experimentally studied a cluster of smaller microparticles bound to a larger one. The observed attractive force could be caused by the plasma flux onto the central particle [48] or ion shadow effects [49].

2. Motion of metallic spheres

The metallic spheres were set into motion relative to the plasma chamber by the cosmonaut shaking the experimental container. The spheres gained momentum when they hit a side wall of the plasma chamber, where they were also reflected. The movie spheres_reflection.avi in the supplemental materials shows reflections and spheres moving through the complex plasma. The sphere motion was not visibly influenced by the plasma or the microparticles.

The microparticles were only visible when they were in the plane formed by the laser sheet. This laser sheet had a full width at half maximum of approximately 80 µm at the focal axis [29]. The spheres reflected much more light than the microparticles due to their larger size. Therefore, they were visible even outside the laser plane, with a depth of field of approximately 8 mm. Whether they were located in front or behind the laser plane can be deduced from two facts: (1) When they were located behind the plane, their image was superposed with images of microparticles. (2) When the spheres were located behind the plane, the side that was not directly illuminated by the laser (the right side in the images) appears brighter than when they were located in front of the plane. This is due to the fact that the sphere reflected more light towards the camera when located behind the laser plane.

Using the motion of the metallic spheres through the laser plane and the fact that the diameter of the spheres is known and much larger than the width of the laser plane, it is possible to estimate their velocity in direction perpendicular to the plane, v_z. Assuming that this velocity does not change during the time interval that the spheres interact with the microparticles and in the absence of external shaking allows estimating the sphere's position in three dimensions. Next, we shall discuss the validity

Table 1. Experimental particulars for the experiments presented below: (1) simple interaction, (2) bubbles, (3) repulsive attraction, and (4) exciting waves. The gas pressure p, velocity of the sphere v_s, Knudsen number Kn, Reynolds number Re, and drag force F_d calculated with (1) are given. In the "exciting waves" experiment (4), a microparticle mixture of diameters 1.55 µm, 2.55 µm, 3.42 µm, 6.8 µm, and 9.19 µm was present, and in all others a mixture of 3.42 µm, 6.8 µm, 9.2 µm, and 14.9 µm. All microparticles except for the 1.55 µm silica particles were composed of melamine formaldehyde with a density of $\rho_\mathrm{d} = 1510\,\mathrm{kg/m^3}$. The table lists the size(s) d_d of those microparticles that are mainly interacting with the sphere during the given experiment.

Exp.	p (Pa)	v_s (mm/s)	Kn	Re (10^{-4})	F_d (nN)	d_d (µm)
(1)	30.0	26.2 ± 1.2	0.5	5.5	3.5 ± 0.3	6.8
(2)	29.0	34.3 ± 1.1	0.5	6.9	4.6 ± 0.3	3.4
(3)	29.3	50.8 ± 12.5	0.5	10.4	7 ± 2	3.4
(4)	15.5	6.0 ± 1.3	0.9	0.65	0.6 ± 0.2	3.4 / 6.8

of that assumption.

2.1. Forces acting on the spheres

The parameters of the spheres moving through the chamber are given in table 1. In the experiments presented here, the spheres move at velocities ranging from 6 mm/s to 50 mm/s. They are relatively large and massive, with a mass $m_\mathrm{s} = 4\pi\rho_\mathrm{s}R^3/3 = 4.1 \times 10^{-6}\,\mathrm{kg}$, where we used a radius of $R = 0.5\,\mathrm{mm}$ and the density of steel, $\rho_\mathrm{s} = 7850\,\mathrm{kg/m^3}$. The metallic spheres are thus 1 to 1000 million times more massive than the microparticles in the plasma.

This large mass means that stopping the sphere from a velocity of $v_\mathrm{s} = 30\,\mathrm{mm/s}$ during a time of $\Delta t = 1\,\mathrm{s}$ would require a force $F_\mathrm{s} = m_\mathrm{s}v_\mathrm{s}/\Delta t = 120\,\mathrm{nN}$.

2.1.1. Microacceleration forces Even though the space station is in free fall, air drag, tidal forces, etc. lead to low frequency microaccelerations, and vibrations from payload and vehicle systems cause high frequency accelerations [53]. Non-negligible quasi steady-state accelerations would lead to a bending of the flight path of the spheres in the plasma chamber. These microaccelerations are measured by the MAMS sensor in the US lab "Destiny" [50]. The data are available for download at the Principle Investigator Microgravity Services website [54].

For the time interval when the present experiment was carried out, the magnitude of the quasi-steady state acceleration was $< 1.0\,\mu g$ except for two counts, where g is the gravitational acceleration at the Earth surface. The PK-3 Plus Laboratory was hosted in the Russian segment of the space station. The extrapolation of the acceleration measurement to other segments is non-trivial and depends on the current motion of the space station [55]. Measurements [55] have shown that a worst case estimate for the magnitude of the microaccelerations in the Russian segment (barring unusual events)

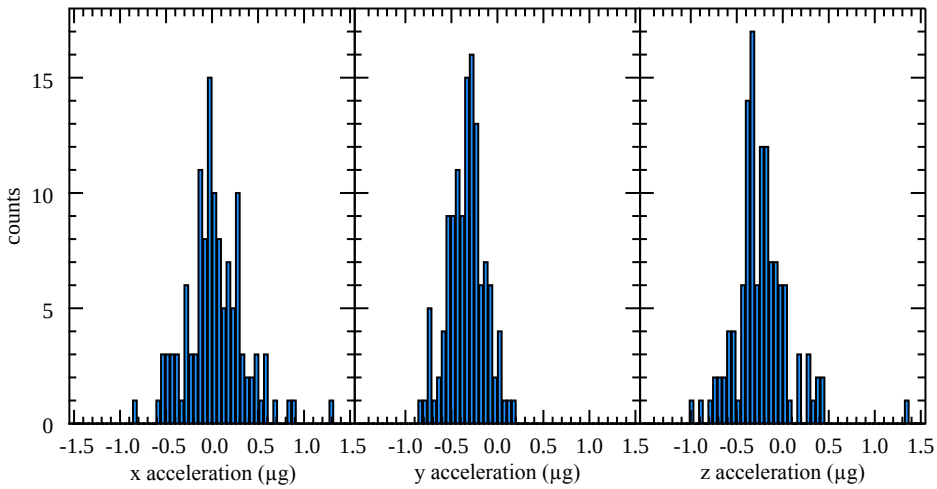

Figure 2. Quasi-steady state acceleration measurements during the time of the experiment presented in this article. The microacceleration was measured every 16 s with the MAMS sensor in the US lab Destiny [50]. The coordinate system is left-handed cartesian. The x direction is oriented along the longitudinal axis of the Destiny module towards the forward direction of the space station, the y direction is down (towards Earth/nadir) at orbital noon, and the z axis completes the coordinate system and is positive in port direction [50–52]. The mean values and their standard deviations are $\langle a_\mathrm{x}\rangle = 0.1 \pm 0.3\,\mu\mathrm{g}$, $\langle a_\mathrm{y}\rangle = -0.3 \pm 0.2\,\mu\mathrm{g}$, and $\langle a_\mathrm{z}\rangle = -0.2 \pm 0.3\,\mu\mathrm{g}$.

is given by that measured by MAMS multiplied with the factor 100; in general, the microaccelerations were comparable in magnitude in both segments.

Let us assume, as upper limit, an acceleration of $a = 100\,\mu\mathrm{g}$ at the location of the PK-3 Plus Laboratory. This results in an effective gravitational force of $F_\mathrm{g,eff} = m_\mathrm{s} a = 4.0\,\mathrm{nN}$, which is two orders of magnitude smaller than the stopping force and thus negligible during the short observation time. Correspondingly, we do not observe any bending of the flight trajectories of the spheres.

2.1.2. Drag force The interaction of spheres immersed in a gas is governed by two dimensionless numbers, the Knudsen number Kn and the Reynolds number Re . The Knudsen number is defined as $Kn = \lambda_\mathrm{mfp}/R$, where λ_mfp is the mean free path of the neutral atoms and $R = 0.5\,\mathrm{mm}$ is the sphere's radius. In the experiments presented here, $\lambda_\mathrm{mfp} = 0.25\,\mathrm{mm}$ to $0.47\,\mathrm{mm}$ [56, 57], which means that $Kn = 0.5$ to 0.9. This puts the experiments in the transitional regime between the free-molecular ($Kn \gg 1$) and continuum ($Kn \ll 1$) regimes.

The Reynolds number is the ratio of inertial to viscous force. It is given by $Re = 2R\rho v_\mathrm{s}/\mu$, with ρ denoting the mass density of the gas, v_s the relative velocity between the gas and the sphere, and μ the gas dynamic viscosity. The dynamic viscosity of argon is $\mu = 2.3 \times 10^{-5}\,\mathrm{kg/m\,s}$ at a gas temperature of $T = 300\,\mathrm{K}$ [56–58]. In the experiments presented here, Re varies from 6.5×10^{-5} to 1.0×10^{-3}. Table 1 gives an overview of the experimental particulars.

In the viscous limit of low Reynolds numbers, the drag force F_d acting on a sphere is given by Stoke's law [59]. When the mean free path of the gas atoms is comparable to or larger than the sphere size, $\lambda_\mathrm{mfp} \geqq R$, the Cunningham slip factor $C(Kn) = 1 + A \cdot Kn$, with a correction parameter A, takes into account slip at the sphere surface [60]. This results in a drag force

$$F_\mathrm{d} = -6\pi\mu R v / C(Kn). \tag{1}$$

The correction parameter A is typically expressed as a functional form [61]

$$A = \alpha + \beta \exp(-\gamma/Kn), \tag{2}$$

where α, β and γ are experimentally measured constants called "slip parameters". To the best of our knowledge, the slip parameters for the transitional regime are not precisely known for gases other than air. It was estimated that the following parameters approximate the parameters in the transition regime in several gases, including argon, to within 5% [57, 62]:

$$\alpha = 1.142, \qquad \beta = 0.558, \qquad \gamma = 0.999. \tag{3}$$

These values of the slip parameters were first measured with a Millikan apparatus by Allen and Raabe [63].

The resulting forces F_d are given in table 1 and are of the order of some nN or less. This makes them at least one to two orders of magnitude smaller than the stopping force F_s estimated above. Thus, during the time intervals that we observe the interaction with the microparticles, the drag force acting on the spheres can be neglected.

2.1.3. Magnus force While moving through the gas, the spheres are slowly spinning. The interaction between spinning sphere and background gas can give rise to a force in transverse direction to the sphere's motion, the Magnus force F_M [64].

At small Reynolds numbers $Re \ll 1$, F_M is given by [65, 66]

$$\boldsymbol{F}_\mathrm{M} = [1 + \mathcal{O}(Re)]\, \pi R^3 m\, n\, \boldsymbol{\omega} \times \boldsymbol{v}, \tag{4}$$

where m is the mass of the gas atoms, and $\mathcal{O}(Re)$ is a correction of the order of the Reynolds number. For the "exciting waves" experiment given in table 1 we estimate an angular velocity of 10 rad/s by observing the rotation of microparticles stuck to the sphere's surface. This results in a force of $F_\mathrm{M} = 6 \times 10^{-6}\,\mathrm{nN}$, which is negligible compared to the drag and stopping forces. Correspondingly, we do not observe any spheres that are not moving in straight lines.

2.1.4. Electric forces All objects immersed in a plasma collect charges. A rule of thumb, based on orbit motion limited (OML) theory [67], gives the charge as

$$Q/e \approx 1400\, T_\mathrm{e}\, a \approx 1.8 \times 10^6, \tag{5}$$

where $T_\mathrm{e} \simeq 2.5\,\mathrm{eV}$ is the electron temperature in eV, and a is the object radius in micrometers [29]. This rule-of-thumb does not take into account ion-neutral collisions

[68, 69] or electron depletion effects [70, 71], and can thus be regarded only as a rough estimate.

In order to obtain an upper limit on the electric force acting on the spheres, we calculate the electric field close to the plasma sheath by using the facts that (i) the plasma electric fields under microgravity and under gravity conditions are the same, and (ii) the microparticles can serve as tracers of the electric field [72]. Under gravity conditions, microparticles are levitated by the sheath electric field. Thus, the magnitude of the electric field E is given by the balance equation

$$m_\mathrm{d} g = q_\mathrm{d} E. \tag{6}$$

Using typical parameters such as those given in table 2 for experiment (1) results in

$$E = m_\mathrm{d} g / q_\mathrm{d} = 1400\,\mathrm{V/m}. \tag{7}$$

The strength of the sheath electric field does not change in microgravity. Thus, we use this magnitude of E to calculate an upper limit of the electric force on the sphere in the plasma bulk as

$$F_\mathrm{E} = Q_\mathrm{s} E = 0.4\,\mathrm{nN}, \tag{8}$$

which is comparable to F_d respectively one order smaller, depending on the parameters. Of course, the strength of the time-averaged electric field increases strongly towards the electrodes. We do, however, not observe a significant deceleration of the spheres before they reach the electrodes, and the sphere movement deep inside the sheath is not relevant for their interaction with the microparticles in any case.

While the sphere is moving through the microparticle cloud, it interacts with the microparticles, which are also charged negatively. Thus, there is an additional force exerted on the sphere due to dissipation in the surrounding microparticle fluid. This additional drag force consists of two parts, an additional contribution to the neutral drag force associated with the neutral gas friction of the surrounding microparticles (the friction-dominated additional drag), and the viscous disspation in the microparticle fluid (the viscosity-dominated additional drag). Ivlev and Zhukhovitskii [73] give the following expression for the additional force on a projectile moving in a complex plasma that induces a subsonic microparticle flow‡

$$F_\mathrm{add} = -4\pi\eta R_\mathrm{eff} v_\mathrm{s} \left(\frac{1 + \tilde{R} + \frac{1}{6}\tilde{R}^2 + \frac{1}{18}\tilde{R}^3}{1 + \frac{1}{3}\tilde{R}} \right), \tag{9}$$

where η is the dynamic shear viscosity of the microparticle fluid, R_eff is the effective projectile radius given by the size of the surrounding cavity in the microparticle cloud, v_s is the projectile velocity, and $\tilde{R} = R_\mathrm{eff}/L_\mathrm{fr}$ with the friction length $L_\mathrm{fr} = \sqrt{\eta/\rho\gamma_\mathrm{Ep}}$. The mass density of the microparticle fluid is denoted by ρ, and the microparticles' friction rate with the background gas by γ_Ep. Using a kinematic viscosity $\nu = \eta/\rho \simeq 5\,\mathrm{mm^2/s}$ [74], a damping rate of $\gamma_\mathrm{Ep} \simeq 55\,\mathrm{s^{-1}}$ [75, 76], and an effective projectile size of

‡ Please note that the spheres move with supersonic velocity in some experiments.

$R_{\text{eff}} = 3.3\,\text{mm}$, which corresponds to experiment (1) in table 1, results in a friction length of $L_{\text{fr}} \simeq 0.3\,\text{mm}$ and a parameter $\tilde{R} \simeq 11$. This gives an additional force

$$F_{\text{add}} \simeq 0.31\,\text{nN}. \tag{10}$$

This additional force on the spheres caused by the interaction with the microparticles is one order of magnitude smaller than the drag force exerted by the neutral gas, and many orders of magnitude smaller than the force required to decelerate the sphere in the space between the top and bottom electrodes.

3. Simple interaction with microparticles

Next we shall consider the forces acting on the microparticles. Table 2 gives the plasma and microparticle parameters for the four experiments we discuss below. The microparticles are strongly influenced by the spheres. This can be seen in figure 3, where a metallic sphere is moving through the laser plane (see also the movie spheres_interaction.avi in the supplemental material). The sphere casts a long shadow on the microparticle cloud (visible as missing microparticles in the image). The microparticles are displaced by the sphere, as the sphere surface is charged negatively like all surfaces in contact with a the plasma.

Figure 4 shows the movement of a sphere and the size of the cavity it produces in the microparticle cloud. The movie spheres_cavity.avi in the supplemental material shows a three-dimensional rotation of the figure. The cavity shape was measured in the

Table 2. Microparticle and plasma parameters for the experiments presented below: (1) Simple interaction, (2) Bubbles, (3) Repulsive attraction, and (4) Exciting waves. The gas pressure p, effective voltage U_{eff}, electron density n_{e} estimated with the scaling parameters in [29], microparticle size d_{d}, microparticle density n_{d} and microparticle charge q_{d} estimated with the drift motion limited theory (DML) [11][a]. Also given are the Havnes parameter $H = q_{\text{d}} n_{\text{d}} / e n_{\text{e}}$ [77], and the microparticle speed of sound c_{d}. The plasma power was 480 mW for all experiments.

Exp.	p (Pa)	U_{eff} (V)	n_{e} (m^{-3})	d_{d} (µm)	n_{d} (m^{-3})	q_{d} (e)	H	c_{d} (mm/s)
(1)	30.0	14.0	5×10^{14}	6.8	1×10^{10} [b]	11000	0.2	5.8
(2)	29.0	13.9	5×10^{14}	3.4	6×10^{10} [b]	5200	0.6	16.0
(3)	29.3	14.0	5×10^{14}	3.4	4×10^{10} [b]	5400	0.4	14.0
(4)	15.5	14.7	3×10^{14}	3.4	30×10^{10} [c]	3600	3.6	19.0
				6.8	20×10^{10} [c]	6600	4.4	9.3

[a] Other theories to estimate the charge are the modified orbital motion limited theory (mOML) [78], and the orbital motion limited theory (OML) [67, 79]. We only give the charge resulting from DML, as all theories result in approximately the same charge for $H < 1$. For $H > 1$, OML is not applicable due to strong electron depletion, while DML and mOML still give about the same charge.
[b] calculated from the position of the first peak of the radial pair correlation function
[c] estimated from the interparticle distance determined by the areal number density

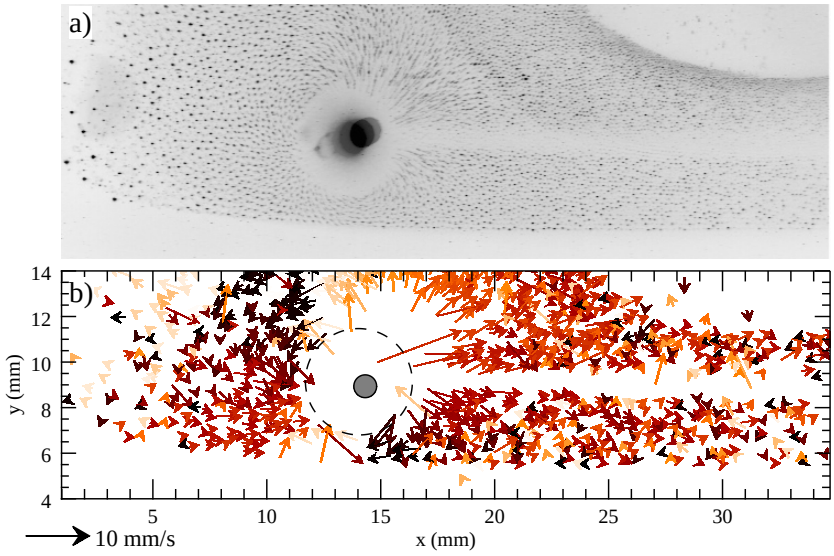

Figure 3. a) Negative of a superposition of three experimental snapshots (field of view: $35 \times 10\,\mathrm{mm}^2$, 40 ms time interval, exp. (1) in table 2) showing a metallic sphere moving in a complex plasma (from bottom left to top right, away from the camera). The sphere is traveling through the laser plane and casts a long shadow on the microparticle cloud (long stripe to the right of the sphere). The microparticles (small dark dots) around the sphere are displaced, forming a cavity in the complex plasma cloud, surrounded by a vortex of particles moving out of the way. A part of the void is visible in the top right. b) Velocity vectors of a subsample of all traced particles corresponding to the middle frame of the three superposed images in (a). The color of the vectors indicates their direction. The movement of the particles around the sphere (gray circle) is well visible. The position of the cavity is indicated as dashed circle.

following way: In the original image, for each pixel we determined whether there were pixels with a high brightness in the surrounding area. Contours were plotted around areas with no bright pixels. We fitted an ellipse [80] to the union of all contours within a cutoff distance from the void center. Figure 4 shows all ellipses in the laser plane as a function of time. The time axis can also be regarded to represent the z direction (perpendicular to the laser plane) in a tomographic manner.

Then, it is possible to estimate the size of the cavity along the sphere trajectory (shown in gray in figure 4). We estimate the distances to the cavity edges by turning the plot shown in figure 4 to a top view and measuring the distances along and perpendicular to the sphere path. We get a distance r_l to the leading edge of the cavity of $r_\mathrm{l} = 3.0\,\mathrm{mm}$, a distance r_t to the trailing edge of $r_\mathrm{t} = 3.5\,\mathrm{mm}$, and a distance $r_\mathrm{f} = 1.8\,\mathrm{mm}$ to the cavity flank/side. This means that the cavity surrounding the sphere is deformed, which is typical for large and fast projectiles moving through a complex plasma [81].

The inset in figure 4 shows the diameter of the cavity in the laser plane as a function of time. The time $t = 0\,\mathrm{s}$ corresponds to the moment when the shadow cast on the microparticle cloud is at its maximum size. After having reached its maximum size, the cavity radius shrinks at a rate of approximately $v_\mathrm{p} = 11\,\mathrm{mm/s}$. Taking into account the angle $\alpha = 40°$ of the trajectory with the laser plane, we calculate the real particle

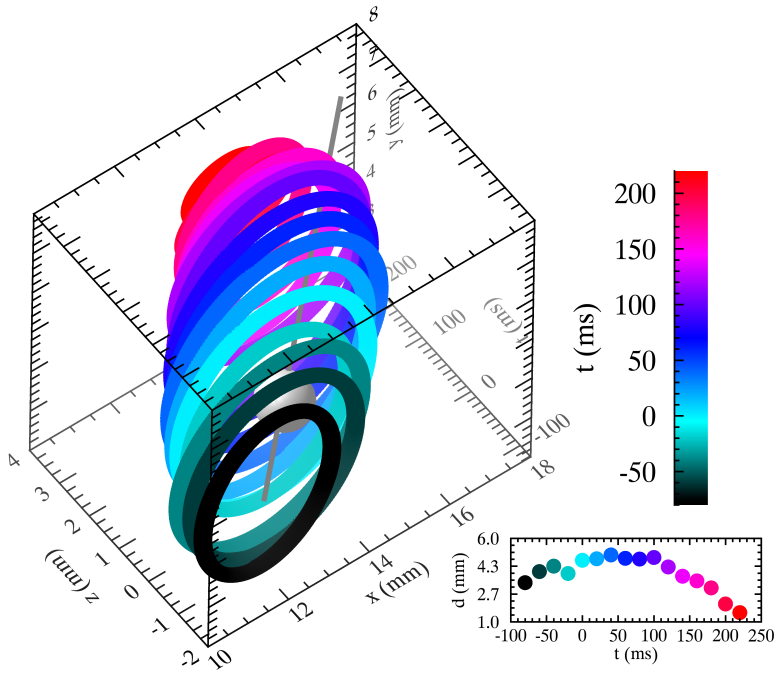

Figure 4. Movement of the sphere shown in Fig. 3 and size of cavity surrounding the sphere. The z position of the sphere is estimated using the assumption that the z-component of its velocity is constant. The sphere trajectory, plotted in gray, forms an angle of approximately 40° with the laser (x,y) plane. The position of the sphere at $t = 0\,\mathrm{s}$, when the shadow it casts on the microparticle cloud is maximal, is indicated as gray ball with 1 mm diameter. The cavity is deformed at larger z positions / later times due to delayed closure. (Inset) Diameter d of the cavity projection on the laser plane as a function of time.

velocity at the cavity edge as $v_\mathrm{r} = \sin\alpha \cdot v_\mathrm{p} = 7.1\,\mathrm{mm/s}$, which is comparable with the speed of sound given in table 2, $c_\mathrm{d} = 5.8\,\mathrm{mm/s}$.

Next, we investigate the force balance acting on the microparticles on the cavity edges, as in [38, 40], see figure 5. First, let us consider the microparticles at the side of the cavity, with a distance from the sphere $r_\mathrm{f} = 1.8\,\mathrm{mm}$. These microparticles are shown in the sketch in figure 5 as filled black circles above and below the sphere. We assume that the microparticle velocity at the side positions is negligible, $v_\mathrm{d} \approx 0$, and thus there is no drag force from movement relative to the neutral gas.

Then, the force balance for a microparticle with mass m_d is (see figure 5)

$$m_\mathrm{d}\frac{d\boldsymbol{v}_\mathrm{d}}{dt} = \boldsymbol{F}_\mathrm{p} + q_\mathrm{d}\boldsymbol{E}(r) + \boldsymbol{F}_\mathrm{i} = 0. \tag{11}$$

$\boldsymbol{F}_\mathrm{p}$ is the pressure force exerted by the microparticle cloud. Its magnitude is given by

$$F_\mathrm{p} \simeq 4\,k_\mathrm{e}\frac{q_\mathrm{d}^2}{\Delta^2}\left(1+\frac{\Delta}{\lambda}\right)e^{-\Delta/\lambda} \simeq 62\,\mathrm{fN}, \tag{12}$$

where $k_\mathrm{e} = 8.99 \times 10^9\,\mathrm{N\,m^2/C^2}$ is Coulomb's constant, $\Delta = 270\,\mu\mathrm{m}$ is the interparticle distance, and $\lambda = \lambda_\mathrm{i} = 54\,\mu\mathrm{m}$ the ion screening length. We assume that the microparticle interacts with four nearest neighbors.

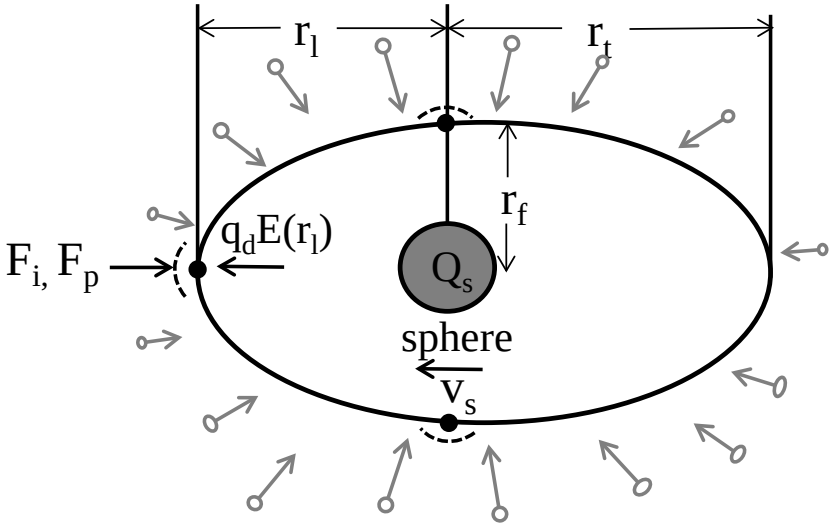

Figure 5. Sketch showing the forces acting on a microparticle at the edges of the cavity. The sphere with charge Q_s is moving towards the left with velocity v_s. The distance from the sphere center to the leading cavity edge is r_1, that to the trailing edge r_t, and that to the flank r_f. Exemplary microparticles with charges q_d are shown as filled black circles. The microparticles are under the action of the sphere's electric field E and the pressure force F_p by the other microparticles in the cloud, indicated as dashed semicircles. The light gray circles indicate ions which are attracted to the negatively charged sphere, exerting an ion drag force on the microparticles.

The sphere charge $Q_\mathrm{s} = 1.8 \times 10^6\,\mathrm{e}$ was estimated in section 2.1.4 with a rule-of-thumb. The electric field it produces is screened inside the cavity with the screening length λ. The electric field strength at position r is given by the derivative of the Yukawa potential,

$$E(r) = k_\mathrm{e}\frac{Q_\mathrm{s}}{r^2}e^{-r/\lambda}\left(1+\frac{r}{\lambda}\right), \tag{13}$$

where Q_s is the sphere charge, r is the distance from the sphere center. The screening length in low temperature plasmas is typically close to the ion Debye length, $\lambda \sim \lambda_\mathrm{i} = 54\,\mu\mathrm{m}$, which is also the screening length we used in calculating the pressure force (12). The ions are strongly accelerated towards the charged sphere. Approximately at a distance of $r = 1.1\,\mathrm{mm}$ from the sphere, the ion velocity becomes larger then their thermal velocity. Under those conditions, the effective screening length approaches the electron Debye length $\lambda_\mathrm{e} = 530\,\mu\mathrm{m}$ [82]. Therefore, we use λ_e as screening length λ inside the cavity. The electric field strength at position $r = r_\mathrm{f} = 1.8\,\mathrm{mm}$ is

$$E(r_\mathrm{f}) = 120\,\mathrm{V/m}, \tag{14}$$

resulting in an electric force

$$q_\mathrm{d}E(r_\mathrm{f}) = 210\,\mathrm{fN}, \tag{15}$$

using the microparticle charge q_d =11 000 e given in table 2. For the ion drag force $\boldsymbol{F}_\mathrm{i}$, we use the expression given by Khrapak et al. [82], which gives F_i for a single

microparticle in a collisionless Maxwellian plasma for an arbitrary ion velocity as

$$F_\mathrm{i} = \sqrt{2\pi} r_\mathrm{d}^2 n_\mathrm{i} m_\mathrm{i} v_\mathrm{Ti}^2 \left\{ \sqrt{\frac{\pi}{2}} \operatorname{erf}\left(\frac{u}{\sqrt{2}}\right) [1 + u + (1 - u^{-2})(1 + 2z\tau) + 4z^2\tau^2 u^{-2} \ln\Lambda] \right.$$
$$\left. + u^{-1}[1 + 2z\tau + u^2 - 4z^2\tau^2 \ln\Lambda] \exp\left(-\frac{u^2}{2}\right) \right\}, \tag{16}$$

where r_d is the microparticle radius, n_i and m_i the ion number density and mass, and $v_\mathrm{Ti} = \sqrt{8k_\mathrm{B}T_\mathrm{i}/\pi m_\mathrm{i}}$ the ion thermal velocity. The ion speed, normalized by the ion thermal velocity, is denoted by u. The dimensionless microparticle charge is given by $z = q_\mathrm{d}|e|/(4\pi\epsilon_0 r_\mathrm{d} k_\mathrm{B} T_\mathrm{e})$, and the ratio of the electron to the ion temperature by $\tau = T_\mathrm{e}/T_\mathrm{i}$. The Coulomb logarithm is given by

$$\ln\Lambda = \ln\left[\frac{\beta + 1}{\beta + (r_\mathrm{d}/\lambda_\mathrm{eff})}\right], \tag{17}$$

with $\beta = q_\mathrm{d}|e|/(4\pi\epsilon_0 k_\mathrm{B} T_\mathrm{i}(1 + u^2)\lambda_\mathrm{eff})$ and the effective screening length $\lambda_\mathrm{eff}(u) = [\lambda_\mathrm{i}^{-2}(1 + u^2)^{-1} + \lambda_\mathrm{e}^{-2}]^{-1/2}$.

The ion velocity can be calculated as a function of the electric field strength E using the ion mobility μ_i, $v_\mathrm{i} = \mu_\mathrm{i} E$. We use the approximation [83]

$$\mu_\mathrm{i}(E) = \frac{\mu_0}{p}\left[1 + \alpha\frac{E}{p}\right]^{-1/2}, \tag{18}$$

with $\mu_0 = 19.5\,\mathrm{m^2\,Pa/V\,s}$, $\alpha = 0.035\,\mathrm{m\,Pa/V}$ for argon ions in argon gas and the gas pressure p in pascal. For the electric field calculated above, $E = 120\,\mathrm{V/m}$, this results in an ion velocity of $v_\mathrm{i} = 73\,\mathrm{m/s}$, directed towards the sphere. Using the parameters above, a plasma density $n_\mathrm{i} = n_\mathrm{e} = 5 \times 10^{14}\,\mathrm{m^{-3}}$, and temperatures $T_\mathrm{i} = 300\,\mathrm{K}$ and $T_\mathrm{e} = 2.5\,\mathrm{eV}$ results in a drag force of

$$F_\mathrm{i}(r_\mathrm{f}) = 110\,\mathrm{fN}, \tag{19}$$

directed towards the sphere.

Thus, the force balance $F_\mathrm{i}(r_\mathrm{f}) + F_\mathrm{p} = q_\mathrm{d} E(r_\mathrm{f})$ holds within 20%. The calculated electric force at the cavity edge is larger than the sum of the ion drag and pressure forces. In order to improve the calculation, the exact variation of the screening length inside the cavity as a function of position might be obtained, and the electric field corrected correspondingly. Also, the charge of the microparticles and of the sphere was approximated, a more precise determination would also improve the accuracy of the force balance. Finally, the uncertainty stems partly from a global ion flow from the center of the plasma chamber to its walls. This flow makes the cavity somewhat asymmetric, see figure 4. In general, a self-consistent simulation of the plasma, microparticles and sphere, including plasma fluxes and charging processes, would shed light on the processes and eventual missing physics, but is beyond the scope of the present paper.

While the cavity is held open by the repulsion from the sphere, its size is determined primarily by the balance between electric force and ion drag force. Once the sphere has left, both ion drag and electric force vanish, and the pressure force F_p closes the cavity.

As F_p is smaller than the other forces, the closure of the cavity is slower than the opening. This explains the cavity deformation visible in figure 4.

Next, we assume that the microparticles at the leading edge of the cavity directly in the sphere's path are displaced with the sphere velocity $v_\mathrm{s} = 26.2$ mm/s. The lengths of the tracks of those particles support that assumption. The force balance at the leading edge r_l is (see figure 5):

$$m_\mathrm{d}\frac{d\boldsymbol{v}_\mathrm{d}}{dt} = \boldsymbol{F}_\mathrm{Ep} + \boldsymbol{F}_\mathrm{p} + \boldsymbol{F}_\mathrm{i} + q_\mathrm{d}\boldsymbol{E}(r_\mathrm{l}), \tag{20}$$

where the drag force exerted by the neutral gas on the microparticle is denoted by F_Ep, and $m_\mathrm{d}d\boldsymbol{v}_\mathrm{d}/dt$ is the deceleration acting on the microparticle. The magnitude of the drag force is

$$F_\mathrm{Ep} = m_\mathrm{d}\gamma_\mathrm{Ep}v_\mathrm{s} \simeq 360\,\mathrm{fN}, \tag{21}$$

with the microparticle mass $m_\mathrm{d} = 2.5 \times 10^{-13}$ kg and the Epstein drag coefficient [76, 84]

$$\gamma_\mathrm{Ep} = 1.48\frac{n_\mathrm{n}m_\mathrm{n}v_\mathrm{th}}{\rho_\mathrm{d}r_\mathrm{d}} = 55\,\mathrm{s}^{-1}, \tag{22}$$

using the number density n_n, atom mass m_n and thermal velocity v_th for argon at a temperature of 300 K, and the parameters given in table 2, experiment (1). The electric field strength $E(r_\mathrm{l}) = 6.7\,\mathrm{V/m}$ results in $q_\mathrm{d}E(r_\mathrm{l}) = 12\,\mathrm{fN}$ and $F_\mathrm{i} = 5.9\,\mathrm{fN}$.

Using the magnitudes of F_p and those given above we can calculate the distance d over which the microparticle decelerate:

$$F_\mathrm{Ep} + F_\mathrm{i} + F_\mathrm{p} - |q_\mathrm{d}|E = m_\mathrm{d}\frac{dv_\mathrm{d}}{dt} = \frac{m_\mathrm{d}v_\mathrm{s}\langle v_\mathrm{d}\rangle}{d} \sim \frac{m_\mathrm{d}v_\mathrm{s}^2}{2d}. \tag{23}$$

Solving for d gives $d = 210\,\mu\mathrm{m}$, which is comparable with the interparticle distance $\Delta = 270\,\mu\mathrm{m}$ measured by using the first peak in the radial pair correlation function $g(r)$, see table 2.

4. Evidence of modified ion flux

It is well known that microparticles, being charged, will modify ion fluxes, bending the ion stream lines and creating space charges in the downstream regions [19, 85–88]. The effect of the highly charged spheres on the ion flux is expected to be more pronounced. Next, we shall highlight some experimental evidence of the modified ion flux.

4.1. Metallic sphere generated bubbles

Figure 6 and the movie spheres_bubble.avi in the supplemental material show a metallic sphere moving vertically with velocity of $v_\mathrm{y} = 30\,\mathrm{mm/s}$ through the microparticle cloud composed of particles of 3.4 µm diameter in an argon plasma at a pressure of 29 Pa. The sphere also has a velocity component in the direction perpendicular to the laser plane (out of the paper plane) of approximately $v_\mathrm{z} = 17\,\mathrm{mm/s}$. Note that, even before the metallic sphere influences the microparticles in the laser plane ($t = 0\,\mathrm{s}$), there is a region of enhanced microparticle density around the void. This "cusp" is commonly

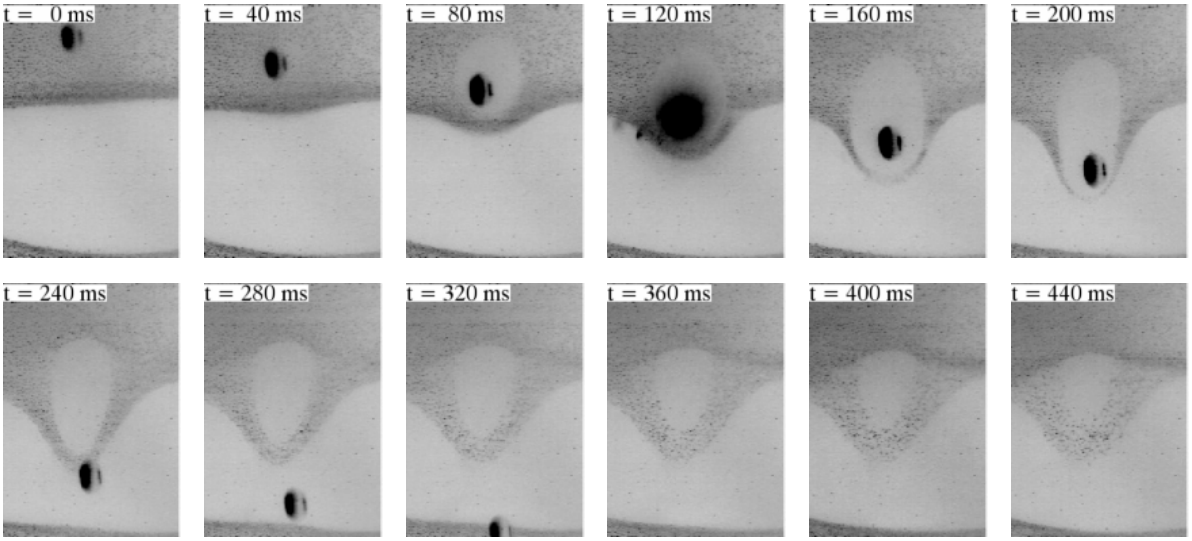

Figure 6. Negative of images with a field of view of $6.5 \times 8.5\,\mathrm{mm}^2$ showing a sphere moving from top to bottom through the void. A bubble around the sphere forms, and microparticles are displaced into the void. Once the sphere has left the vicinity of the void edge, the bubble loses cohesion, and the microparticles slowly move back towards the void edge.

observed in complex plasmas under microgravity conditions [25, 89] and might be explained with dust invariants [89] or a change in the direction of the ion flow [90]. At $t = 40\,\mathrm{ms}$ to 80 ms, when the metallic sphere approaches the void edge downwards from inside the cloud, it pushes the cusp into the void, forming a bubble in the microparticle fluid, compare figure 6. This bubble resembles well the "secondary void" observed by Klindworth et al. [91] forming around a negatively biased Langmuir probe inside a microparticle void during a parabolic flight. The bubble reminds visually of bubbles observed in the microparticle cloud near the void under the influence of thermophoresis [92]. Then, their formation was attributed to a flux of the neutral gas induced by the temperature gradient and to an effective surface tension caused by ions streaming to the microparticle bubble [92, 93].

Note also that the microparticles in the cusp region of the bubble are not simply pushed into the void. Instead, they move inside the bubble wall back towards the main microparticle cloud, gradually thinning the bubble out. It can reasonably be interpreted to indicate the presence of an effective surface tension, as in [92]. This effective surface tension is caused by ion drag acting on the microparticles at intermediate distances. The force balance is as found in [37] – at small distances, the microparticles are repelled, at large distances, attracted by the metallic sphere due to the interplay of electric and ion drag forces.

In [92], the effective surface tension α of the bubbles was estimated as the total mass M of all microparticles moved during the breakup of the bubble in time τ, $\alpha \simeq M/\tau^2$. Here, we can estimate M from the change in the width of the bubble wall in time τ, assuming that the microparticle density in the cusp is about twice that in the main

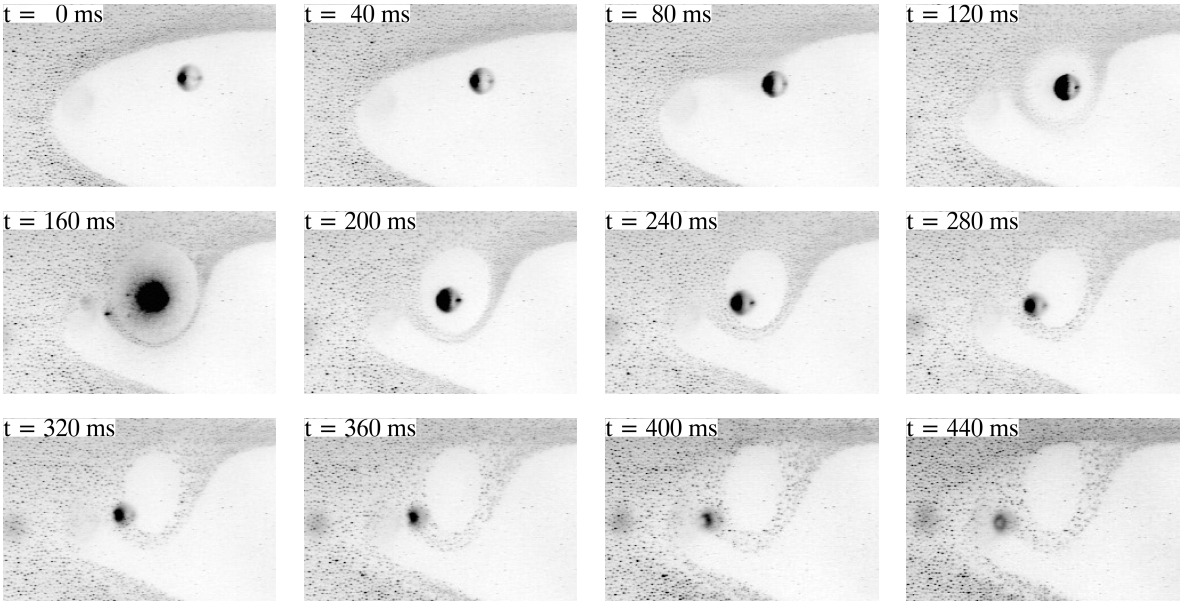

Figure 7. A metallic sphere is moving inside the void of a complex plasma cloud. The original images with a field of view of $11.9 \times 7.2\,\mathrm{mm}^2$ were inverted, and the contrast was adjusted. The sphere is moving simultaneously from right to left and perpendicular to the field of view. When it approaches the void boundary ($t = 80\,\mathrm{ms}$), the particles in the complex plasma cloud move towards the sphere, forming a bubble around it ($t = 120\,\mathrm{ms}$). The sphere crosses the laser plane at $t = 160\,\mathrm{ms}$ (its image is overexposed). After the sphere has left the laser plane, the bubble loses cohesion, and the microparticles slowly fall back towards the main cloud. See supplemental material for a movie.

microparticle cloud, as determined in [89]. This results in an effective surface tension $\alpha \approx 4 \times 10^{-11}\,\mathrm{kg/s^2}$, which is about 1/2 to 1/3 of that determined in [92] for the same microparticle size and a gas pressure of only 18 Pa compared to 30 Pa in the present experiment. Note that this value is many orders of magnitude smaller than that predicted in [94] where the effective surface tension caused by ion wakes was calculated.

After the sphere has left the vicinity of the bubble, the bubble loses cohesion, and the microparticles start to slowly drift back to the main cloud. This shows that once there is no more ion flux towards a sphere in the laser plane, the effective surface tension vanishes, and the ions follow the ordinary force field inside the void [95].

4.2. Repulsive attraction

Let us test the hypothesis of an attractive interaction at intermediate distances from the metallic spheres by considering a sphere traveling inside the void, initially far from the cloud edge. When the sphere approaches the microparticles, we expect them to first move towards the sphere and then be repelled at small distances. We term this behavior "repulsive attraction", as the sphere and the microparticles all are charged negatively and normally have to repel each other. Repulsive attraction between like-charged particles in a complex plasma has been observed before, for instance in the case

of droplet formation [92] and boundary-free clusters [48].

Figure 7 and the movie spheres_attraction.avi in the supplemental materials show exactly this expected behavior: A metallic sphere moves inside the void along the cloud edge. When it gets close to the edge, the microparticles move towards and around it, forming a bubble inside the void.

The counter-intuitive repulsive attraction is due to the change in the electric potential and ion flux caused by the metallic sphere. The position of the void edge is determined by a balance of the ion drag force, directed outwards, and the electric force, directed inwards. When the strongly charged sphere approaches the void edge, it changes the balance of forces, leading to a new microparticle equilibrium position. After the sphere has left the vicinity, the microparticle bubble again loses cohesion, as discussion in section 4.1, and the microparticles slowly drift back to the main cloud.

4.3. Exciting waves

Dust-density waves (DDWs) are spontaneously excited in complex plasmas by an ion-microparticle streaming instability [72, 96, 97]. They typically follow the local ion flux, but can also move obliquely [98]. They are strongly influenced by objects in the cloud, for instance, Choudhary et al. [99] found that a floating rod in a DC glow discharge modifies the local electric field, which in turn alters the ion flow and thus the direction of DAWs – in the presence of the rod, the waves propagate obliquely, and Kim et al. [100] observed a similar distortion of wave ridges flowing around a glass rod in DC glow discharge, which they explained in terms of diffraction of waves around an obstacle.

Dust waves are excited when the microparticle density is high enough, the gas pressure low enough and the local electric field large enough to accelerates the ions above a threshold streaming velocity. This condition can be expressed in terms of the local electric field [72] or in terms of the position of the dust cloud with respect to the sheath [101]. An approximation for the critical electric field for wave excitation is [102]

$$E_{\mathrm{cr}} = \frac{\gamma_{\mathrm{Ep}}}{c_{\mathrm{d}}} \frac{k_{\mathrm{B}} T_{\mathrm{i}}}{e}, \tag{24}$$

where γ_{Ep} is the gas damping rate, c_{d} the microparticles' speed of sound, T_{i} is the ion temperature, k_{B} is Boltzmann's constant, and e the elementary charge.

In the present experiment, DDWs were excited by the spheres in a region of the microparticle cloud where conditions are close to the excitation threshold. Figure 8 shows a sphere moving through a complex plasma in argon at a pressure of 15.5 Pa and an effective voltage of 14.7 V. The complex plasma was formed of a mixture of particles of sizes between 1.55 µm and 9.19 µm, which arrange around the void ordered by size. The sphere is mainly interacting with particles of sizes 3.4 µm and 6.8 µm. The microparticles at the left side of the plasma are undergoing self-excited waves. The sphere approaches the active region from the right and from behind, moving in a part of the cloud that is not undergoing wave activity (t = 0.0 s to 0.4 s). In the vicinity of the active region (t = 0.8 s), waves appear once the sphere gets close. This is

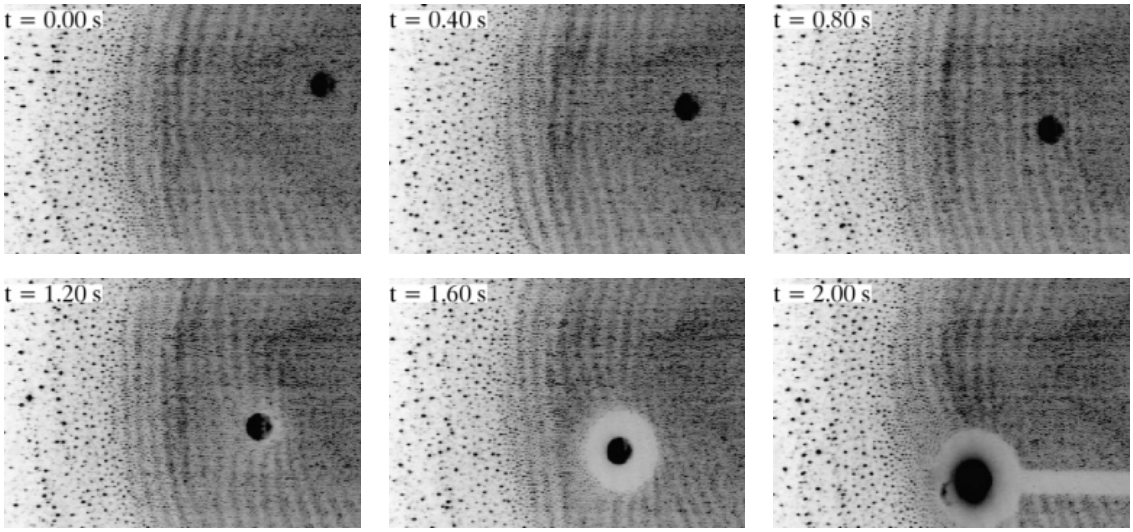

Figure 8. Experimental images showing a metallic sphere that moves through a complex plasma cloud with self-excited waves. The original images with a field of view of $16 \times 9\,\mathrm{mm}^2$ were inverted. First, the sphere is located outside the laser plane illuminating the microparticles. When it approaches the plane ($t = 0.8\,\mathrm{s}$), it induces waves in a region of the plasma cloud that was previously quiescent. As the sphere moves into the laser plane, it repels the microparticles, so that a cavity forms around the sphere. The wave ridges become visibly bent near the cavity surface. The sphere reaches the center of the laser plane at $t = 2\,\mathrm{s}$, where it casts an extended horizontal shadow. At that time, the wave ridges orient perpendicular to the cavity surface. See Supplemental Material for a movie.

expected behavior, as the strong electric field of the metallic sphere will accelerate ions in addition to the chamber's background electric field. The wave ridges also get visible bent towards the sphere ($t = 1.2\,\mathrm{s}$ to $2.0\,\mathrm{s}$), indicating the direction of the ion flow that is bent around the sphere. The corresponding movie is available in the supplemental material (spheres_waves.avi).

Under these conditions, the critical field (24) is

$$E_{\mathrm{cr}} \simeq 80\,\mathrm{V/m}, \tag{25}$$

for both particle sizes ($r_{\mathrm{d}} = 1.7\,\mu\mathrm{m}$, $c_{\mathrm{d}} = 19\,\mathrm{mm/s}$, $\gamma_{\mathrm{Ep}} = 57\,\mathrm{s}^{-1}$ resp. $r_{\mathrm{d}} = 3.4\,\mu\mathrm{m}$, $c_{\mathrm{d}} = 9.3\,\mathrm{mm/s}$, and $\gamma_{\mathrm{Ep}} = 29\,\mathrm{s}^{-1}$, compare table 2). In the vicinity of the active region, the discharge electric field is already almost strong enough to reach the critical electric field. When the sphere approaches, its electric field is added to the discharge field, and the total field magnitude then crosses the threshold.

In comparison, for the experiments with pressures $p \simeq 30\,\mathrm{Pa}$ discussed in sections 3, 4.1, and 4.2, the critical electric field is $E_{\mathrm{cr}} = 180\,\mathrm{V/m}$ to $250\,\mathrm{V/m}$, which is larger than the sum of the sphere and discharge electric fields. Correspondingly, the microparticle clouds in those experiments were not undergoing wave activity.

5. Summary

We presented the first experiments on the interaction between a complex plasma and metallic spheres of 1 mm diameter under microgravity conditions. The spheres were set into motion when the experimental container was shaken and they hit the chamber walls. While the microparticles were trapped in the plasma, the motion of the spheres was almost force-free: The drag forces, microaccelerations and electric forces acting on the spheres were negligible during the interaction time with the microparticles.

The influence of the spheres on the microparticles and the local plasma environment was profound. The spheres acquired high electric charges of the order of 1.8×10^6 e and were surrounded by microparticle-free cavities with diameters of a few millimeters. The position of the cavity edge is determined by an interplay of the electric, pressure and ion drag forces, as well as inertia and neutral drag force if the microparticles are moving. For stationary microparticles at the cavity edge, the force balance between the electric force, ion drag force and pressure force from other microparticles holds to within 20%, using the electron Debye length as screening length inside the cavity, and neglecting the global ion flux. We showed that the spheres strongly influenced the ion motion, leading to an effective attraction of microparticles to the spheres at intermediate distances, to an effective surface tension $\alpha \sim 4 \times 10^{-11}\,\mathrm{kg/s^2}$, and to the excitation of dust density waves by increasing the local electric field strength above the threshold field necessary to trigger the waves ($E_{\mathrm{cr}} = 80\,\mathrm{V/m}$ to $250\,\mathrm{V/m}$ under the conditions of the given experiments).

We covered a range of pressures and interaction scenarios in the experiments presented here. In the future, we plan a more detailed and thorough investigation of interaction effects such as wave excitation. Experiments under gravity conditions where spheres are dropped through a complex plasma cloud [103–105] could complement the study presented here and would allow comparing the effects of spheres made of various materials.

Acknowledgments

We would like to thank Ingo Laut for carefully checking the manuscript, and Dr. Alexei Ivlev and Dr. Vladimir Nosenko for helpful comments. We also thank the PIMS project/NASA for providing the microacceleration data. The PK-3 Plus project was funded by the space agency of the Deutsches Zentrum für Luft- und Raumfahrt eV with funds from the Federal Ministry for Economy and Technology according to a resolution of the Deutscher Bundestag under grant number 50 WM 1203. A. M. Lipaev, V. I. Molotkov and V. N. Naumkin are supported by the Russian Science Foundation Grant No. 14-12-01235.

References

[1] Morfill G E, Ivlev A V and Thomas H M 2012 *Phys. Plasmas* **19** 055402

[2] Poppe T, Blum J and Henning T 2000 *Astrophys. J.* **533** 472

[3] Lee V, Waitukaitis S R, Miskin M Z and Jaeger H M 2015 *Nature Phys.* **11** 733–737

[4] Ivlev A V, Akimkin V V and Caselli P 2016 *Astrophys. J.* **833** 92

[5] Okuzumi S 2009 *Astrophys. J.* **698** 1122

[6] Okuzumi S, Tanaka H and Sakagami M 2011 *Astrophys. J.* **731** 95; Okuzumi S, Tanaka H, Takeuchi T and Sakagami M 2011 *Astrophys. J.* **731** 96

[7] Tsytovich V N, Ivlev A V, Burkert A and Morfill G E 2013 *Astrophys. J.* **780** 131

[8] Shukla P K and Mamun A A 2002 *Introduction to Dusty Plasma Physics* (Bristol: Institute of Physics Publishing)

[9] Morfill G E and Ivlev A V 2009 *Rev. Mod. Phys.* **81** 1353

[10] Akdim M R and Goedheer W J 2003 *Phys. Rev. E* **67** 056405

[11] Morfill G E, Konopka U, Kretschmer M, Rubin-Zuzic M, Thomas H M, Zhdanov S K and Tsytovich V 2006 *New J. Phys.* **8** 7

[12] Rubin-Zuzic M, Morfill G E, Thomas H M, Ivlev A V, Klumov B A, Rothermel H, Bunk W, Pompl R, Havnes O and Fouquét A 2006 *Nature Physics* **2** 181

[13] Piel A, Klindworth M and Melzer A 2008 *Phys. Rev. E* **77** 026407

[14] Heidemann R, Zhdanov S, Sütterlin K R, Thomas H M and Morfill G E 2011 *EPL* **96** 15001

[15] Schwabe M and Graves D B 2013 *Phys. Rev. E* **88** 023101

[16] Melzer A 2014 *Phys. Rev. E* **90** 053103

[17] Tsai Y Y, Tsai J Y and I L 2016 *Nature Phys.* **12** 573–577

[18] Schwabe M, Zhdanov S and Räth C 2017 *Phys. Rev. E* **95** 041201(R)

[19] Kompaneets R, Morfill G E and Ivlev A V 2016 *Phys. Rev. E* **93** 063201

[20] Goree J, Morfill G E, Tsytovich V N and Vladimirov S V 1999 *Phys. Rev. E* **59** 7055–7067

[21] Fortov V E, Nefedov A P, Vaulina O S, Lipaev A M, Molotkov V I, Samaryan A A, Nikitskii V P, Ivanov A I, Savin S F, Kalmykov A V, ev A Y S and Vinogradov P V 1998 *J. Exp. Theo. Phys.* **87** 1087–1097

[22] Thomas H M, Morfill G E, Fortov V E, Ivlev A V, Molotkov V I, Lipaev A M, Hagl T, Rothermel H, Khrapak S A, Sütterlin R K, Rubin-Zuzic M, Petrov O F, Tokarev V I and Krikalev S K 2008 *New J. Phys.* **10** 033036

[23] Molotkov V I, Thomas H M, Lipaev A M, Naumkin V N, Ivlev A V and Khrapak S A 2015 *Int. J. Microgravity Sci. Appl.* **3** 320302

[24] Khrapak A G, Molotkov V I, Lipaev A M, Zhukhovitskii D I, Naumkin V N, Fortov V E, Petrov O F, Thomas H M, Khrapak S A, Huber P, Ivlev A and Morfill G 2016 *Contrib. Plasma Phys.* **56** 253–262

[25] Lipaev A M, Khrapak S A, Molotkov V I, Morfill G E, Fortov V E, Ivlev A, Thomas H M, Khrapak A G, Naumkin V N, Ivanov A I, Tretschev S E and Padalka G I 2007 *Phys. Rev. Lett.* **98** 265006

[26] Ivlev A V, Morfill G E, Thomas H M, Räth C, Joyce G, Huber P, Kompaneets R, Fortov V E, Lipaev A M, Molotkov V I, Reiter T, Turin M, Vinogradov P 2008 *Phys Rev Lett* **100** 095003

[27] Schwabe M, Zhdanov S K, Thomas H M, Ivlev A V, Rubin-Zuzic M, Morfill G E, Molotkov V I, Lipaev A M, Fortov V E, and Reiter T 2008 *New J Phys* **10** 033037

[28] Sütterlin K R, Wysocki A, Ivlev A V, Räth C, Thomas H M, Rubin-Zuzic M, Goedheer W J, Fortov V E, Lipaev A M, Molotkov V I, Petrov O F, Morfill G E, and Löwen H 2009 *Phys Rev Lett* **102** 085003

[29] Heidemann R J, Couëdel L, Zhdanov S K, Sütterlin K R, Schwabe M, Thomas H M, Ivlev A V, Hagl T, Morfill G E, Fortov V E, Molotkov V I, Petrov O F, Lipaev A I, Tokarev V, Reiter T, Vinogradov P 2011 *Phys Plasmas* **18** 053701

[30] Khrapak S A, Klumov B A, Huber P, Molotkov V I, Lipaev A M, Naumkin V N, Ivlev A V, Thomas H M, Schwabe M, Morfill G E, Petrov O F, Fortov V E, Malentschenko Yu, and Volkov S 2012 *Phys. Rev. E* **85** 066407

[31] Zhdanov S, Schwabe M, Räth C, Thomas H M, Morfill G E 2015 *EPL* **110** 35001

[32] Yang L, Schwabe M, Zhdanov S, Thomas H M, Lipaev A M, Molotkov V I, Fortov V E, Zhang J, Du C-R 2017 *EPL* **117** 25001

[33] Dunaevsky A, Raitses Y and Fisch N J 2003 *Phys. Plasmas* **10** 2574

[34] Pavlů J, Šafránková J, Němeček Z and Richterová I 2009 *Contrib. Plasma Phys.* **49** 169

[35] Law D A, Steel W H, Annaratone B M and Allen J E 1998 *Phys. Rev. Lett.* **80** 4189–4192

[36] Thompson C O, D'Angelo N and Merlino R L 1999 *Phys. Plasma* **6** 1421

[37] Samsonov D, Ivlev A V, Morfill G E and Goree J 2001 *Phys. Rev. E* **63** 025401(R)

[38] Thomas Jr E, Avinash K and Merlino R L 2004 *Phys. Plasmas* **11** 1770

[39] Klindworth M, Arp O and Piel A 2007 *Rev. Sci. Instrum.* **78** 033502

[40] Harris B J, Matthews L S and Hyde T W 2015 *Phys. Rev. E* **91** 063105

[41] Jiang K, Nosenko V, Li Y F, Schwabe M, Konopka U, Ivlev A V, Fortov V E, Molotkov V I, Lipaev A M, Petrov O F, Turin M V, Thomas H M and Morfill G E 2009 *EPL* **85** 45002

[42] Arp O, Caliebe D and Piel A 2011 *Phys. Rev. E* **83** 066404

[43] Caliebe D, Arp O and Piel A 2011 *Phys. Plasmas* **18** 073702

[44] Schwabe M, Jiang K, Zhdanov S, Hagl T, Huber P, Ivlev A V, Lipaev A M, Naumkin V N, Sütterlin K R, Thomas H M, Fortov V E, Morfill G E, Skvortsov A and Volkov S 2011 *EPL* **96** 55001

[45] Basner R, Sigeneger F, Loffhagen D, Schubert G, Fehske H, and Kersten H 2009 *New J Phys* **11** 013041

[46] Schubert G, Haass M, Trottenberg T, Fehske H, and Kersten H 2012 *Contrib Plasma Phys* **52**, 827

[47] Uchida G, Iizuka S, Kamimura T and Sato N 2009 *Phys. Plasmas* **16** 053707

[48] Usachev A D, Zobnin A, Petrov O F, Fortov V E, Annaratone B M, Thoma M H, Höfner H, Kretschmer M, Fink M and Morfill G E 2009 *Phys. Rev. Lett.* **102** 045001

[49] Lampe M and Joyce G 2015 *Phys. Plasmas* **22** 023704

[50] Jules K, Hrovat K, Kelly E, McPherson K, Reckart T, and Grodsinksy C 2002 *NASA Tech. Rep.* **NASA/TM-2002-211693**

[51] NASA International Space Station Program, Space Station Reference Coordinate Systems – SSP 30219 Revision F, 2001

[52] McPherson K M 2002 *PIMS Acceleration Data File Description Document* **PIMS-ISS-001**

[53] European Space Agency: European User Guide to Low Gravity Platforms 2015 *online* `http://www.esa.int/Our_Activities/Human_Spaceflight/Research/European_user_guide_to_low_gravity_platforms`, accessed on 21 July 2017

[54] NASA: Principle Investigator Microgravity Services *online* `https://pims.grc.nasa.gov/pims_iss_index.html`, accessed on 21 July 2017

[55] Putin G F, Glukhov A F, Babushkin I A, Zavalishin D A, Belyaev M Yu, Ivanov A I, and Sazonov V V 2012 *Cosmic Research* **50** 373

[56] Baron P A and Willeke K 1993 *Aerosol Measurement* (New York: Van Nostrand Reinhold) chap Gas and Particle Motion, pp 23–40

[57] Schmid O, Trueblood M B, Gregg N, Hagen D E and Whitefield P D 2002 *Aerosol Sci. Techn.* **36** 351–360

[58] Kestin J, Ro S T and Wakeham W A 1972 *J. Chem. Phys.* **56** 4119

[59] Stokes G G 1851 *Trans. Cambridge Phil. Soc.* **9** 8–106

[60] Cunningham E 1910 *Proc. Roy. Soc. A* **83** 357

[61] Knudsen M and Weber S 1911 *Ann. Phys.* **36** 981–994

[62] Rader D J 1990 *J. Aerosol Sci.* **21** 161–168

[63] Allen M D and Raabe O G 1985 *Aerosol Sci Technol* **4** 269

[64] Volkov A N 2009 *Fluid Dynamics* **44** 141–157

[65] Rubinow S I and Keller J B 1961 *J. Fluid Mech.* **11** 447

[66] Borg K I, Söderholm L H and Essén H 2003 *Phys. Fluid* **15**

[67] Mott-Smith H and Langmuir I 1926 *Phys. Rev* **28** 727

[68] Zobnin A V, Nefedov A P, Sinel'shchikov V A and Fortov V E 2000 *J. Exp. Theor. Phys.* **91** 483–487

[69] Hutchinson I H and Patacchini L 2007 *Phys. Plasmas* **14** 013505

[70] Samsonov D, and Goree J 1999 *Phys Rev E* **59** 1047

[71] Goertz I, Greiner F, and Piel A 2011 *Phys Plasmas* **18** 013703

[72] Merlino R L 2009 *Phys Plasmas* **16** 124501

[73] Ivlev A V and Zhukhovitskii D I 2012 *Phys. Plasmas* **19** 093703

[74] Schwabe M, Zhdanov S, Räth C, Graves D B, Thomas H M and Morfill G E 2014 *Phys. Rev. Lett.* **112** 115002

[75] Epstein P 1924 *Phys. Rev.* **23** 710–733

[76] Konopka U 2000 *Wechselwirkungen geladener Staubteilchen in Hochfrequenzplasmen* Ph.D. thesis Ruhr-Universität-Bochum

[77] Havnes O, Morfill G E and Goertz C K 1984 *J. Geophys. Res.* **89** 10999–11003

[78] Khrapak S A, Ratynskaia S V, Zobnin A V, Usachev A D, Yaroshenko V V, Thoma M H, Kretschmer M, Höfner H, Morfill G E, Petrov O F and Fortov V E 2005 *Phys. Rev. E* **72** 016406

[79] Bonitz M, Henning C and Block D 2010 *Rep. Prog. Phys.* **73** 066501

[80] Markwardt C 2017 Markwardt idl library online URL `http://cow.physics.wisc.edu/%7ecraigm/idl/idl.html`

[81] Zhukhovitskii D I, Ivlev A V, Fortov V E and Morfill G E 2013 *Phys. Rev. E* **87** 063108

[82] Khrapak S A, Ivlev A V, Zhdanov S K and Morfill G E 2005 *Phys. Plasmas* **12** 042308

[83] Frost L S 1956 *Phys. Rev.* **105** 354–356

[84] Epstein P S 1929 *Z. Physik A* **54** 537–563

[85] Vladimirov S V and Nambu M 1995 *Physical Review E* **52** R2172–R2174

[86] Melandsø F and Goree J 1995 *Phys. Rev. E* **52** 5312–5326

[87] Melzer A, Schweigert V A and Piel A 1999 *Phys. Rev. Lett.* **83** 3194 3197

[88] Miloch W J, Trulsen J and Pécseli H L 2008 *Phys. Rev. E* **77** 056408

[89] Naumkin V N, Zhukhovitskii D I, Molotkov V I, Lipaev A M, Fortov V E, Thomas H M, Huber P and Morfill G E 2016 *Phys. Rev. E* **94** 033204

[90] Gozadinos G, Ivlev A V and Boeuf J P 2003 *New J. Phys.* **5** 32

[91] Klindworth M, Piel A, Melzer A, Konopka U, Rothermel H, Tarantik K and Morfill G E 2004 *Phys. Rev. Lett.* **93** 195002

[92] Schwabe M, Rubin-Zuzic M, Zhdanov S, Ivlev A V, Thomas H M and Morfill G E 2009 *Phys. Rev. Lett.* **102** 255005

[93] Schwabe M, Hou L J, Zhdanov S, Ivlev A V, Thomas H M and Morfill G E 2011 *New J. Phys.* **13** 083034

[94] Bashkirov A G 2004 *Phys. Rev. E* **69** 046410

[95] Kretschmer M, Khrapak S A, Zhdanov S K, Thomas H M, Morfill G E, Fortov V E, Lipaev A M, Molotkov V I, Ivanov A and Turin M 2005 *Phys. Rev. E* **71**

[96] Barkan A, Merlino R L and D'Angelo N 1995 *Phys. Plasmas* **2** 3563–3565

[97] Rosenberg M 1996 *J. Vac. Sci. Technol. A* **14** 631–633

[98] Piel A, Klindworth M, Arp O, Melzer A and Wolter M 2006 *Phys. Rev. Lett.* **97** 205009

[99] Choudhary M, Mukherjee S and Bandyopadhyay P 2016 *Phys. Plasmas* **23**

[100] Kim S H, Heinrich J R and Merlino R L 2008 *Phys. Plasmas* **15** 090701

[101] Schwabe M, Rubin-Zuzic M, Zhdanov S, Thomas H M and Morfill G E 2007 *Phys. Rev. Lett.* **99** 095002

[102] Fink M A, Zhdanov S K, Schwabe M, Thoma M H, Höfner H, Thomas H M and Morfill G E 2013 *EPL* **102** 45001

[103] Zafiu C, Melzer A, and Piel A 2002 *Phys Plasmas* **9** 1278

[104] Nosenko V, Fisher R, Merlino R, Khrapak S, Morfill G, Avinash K 2007 *Phys. Plasmas* **14** 103702

[105] Dropmann M, Chen M, Sabo H, Laufer R, Herdrich G, Matthews L S, and Hyde T W 2016 *J Plasma Phys* **82** 615820401